



Positions of Ocular Geometrical and Visual Axes in Brazilian, Chinese and Italian Populations

Ahmed Abass, Riccardo Vinciguerra, Bernardo T Lopes, FangJun Bao, Paolo Vinciguerra, Renato Ambrósio & Ahmed Elsheikh

To cite this article: Ahmed Abass, Riccardo Vinciguerra, Bernardo T Lopes, FangJun Bao, Paolo Vinciguerra, Renato Ambrósio & Ahmed Elsheikh (2018): Positions of Ocular Geometrical and Visual Axes in Brazilian, Chinese and Italian Populations, Current Eye Research, DOI: [10.1080/02713683.2018.1500609](https://doi.org/10.1080/02713683.2018.1500609)

To link to this article: <https://doi.org/10.1080/02713683.2018.1500609>



Accepted author version posted online: 14 Jul 2018.



Submit your article to this journal [↗](#)



Article views: 1



View Crossmark data [↗](#)

Positions of ocular geometrical and visual axes in Brazilian, Chinese and Italian populations

Ahmed Abass^{1*}, Riccardo Vinciguerra², Bernardo T Lopes^{1,6}, FangJun Bao³, Paolo Vinciguerra⁴⁻⁵, Renato Ambrósio Jr⁶, Ahmed Elsheikh^{1,7}

¹ School of Engineering, University of Liverpool, Liverpool, UK

² Royal Liverpool and Broadgreen University Hospital, Liverpool, UK.

³ Eye Hospital, WenZhou Medical University, WenZhou Shi, China

⁴ Departement of Biomedical Science, Humanitas University, Rozzano (MI), Italy.

⁵ Eye Center, Humanitas Clinical and Research Center, Rozzano (MI), Italy.

⁶ Universidade Federal de São Paulo, São Paulo, Brazil

⁷ National Institute for Health Research (NIHR) Biomedical Research Centre at Moorfields Eye Hospital NHS Foundation Trust and UCL Institute of Ophthalmology, London, UK

* Corresponding author:

Ahmed Abass

School of Engineering, University of Liverpool, Liverpool, L69 3GH, UK.

A.Abass@liverpool.ac.uk

Keywords: cornea; topography; optical axis; visual axis; levelling the eye

Number of words: 4518

Abstract

Purpose: To identify the relative positions of geometrical and visual axes of the eye and present a method to locate the visual centre when the geometrical axis is taken as a reference.

Methods: Topography elevation data was collected using a Pentacam HR[®] topographer from 2040 normal eyes of 1020 healthy participants in Brazil, China and Italy. A

three-dimensional, rotation algorithm, a first-order Zernike polynomial fit and a nonlinear least-squares error function was used within an optimisation function to locate the geometrical axis and the visual centre of each eye.

Results: The right eyes of participants were significantly more tilted than left eyes throughout the topography scanning process ($p < 0.001$). The visual centres were always located in the nasal-superior quadrant, although the visual centres of fellow eyes were not symmetrically located. Mean distances between the visual centre and the geometrical centre in right eyes were 0.8 ± 0.29 mm, 0.56 ± 0.18 mm, and 0.91 ± 0.34 mm among Brazilian, Chinese, and Italian participants, respectively, and located at angular positions of $38.7 \pm 24.5^\circ$, $23.0 \pm 29.8^\circ$ and $23.1 \pm 28.1^\circ$ from the nasal side. However, in left eyes, mean distances were 0.76 ± 0.33 mm, 0.45 ± 0.12 mm and 0.75 ± 0.33 mm at polar angles from the nasal side of $59.3 \pm 29.0^\circ$, $50.6 \pm 44.5^\circ$ and $61.8 \pm 34.1^\circ$, respectively.

Conclusions: Fellow eyes do not perform similarly during the fixation process, with right eyes tending to tilt more than left eyes, and the visual centres of the fellow eyes positioned differently relative to the geometrical centres.

Introduction

As the visual acuity is tested by Snellen chart at a six-meter distance to simulate the focus on distant objects at infinity while keeping the fellow eyes parallel (1), this is not the case when scanning corneal topography. When the surface of the eye is being reconstructed by a videokeratography topographer, the target fixation target is positioned within the device's head close to the eye, which stimulate accommodation and convergence. Some modern eye scanners have limited adjustable virtual fixation target systems. The Pentacam HR, as an example, has a red blinking Light Emitting Diode (LED) that virtually serves as a movable

fixation target that moves virtually in half dioptre steps, but with limited range of 2.0 to -5.0 dioptres (2), which is still insufficient to stimulate accommodation and convergence. Therefore, fixation on an object, such as a topographer's focusing target, at a short distance requires a response from the ocular system to achieve a clear focused vision (3). Besides the convergence, another source of misalignment between the optical and the visual axis, is foveal position, its centre is not placed on the optical axis, but located around 3.4 mm temporal to the optic disk edge (4), 2.5 mm temporal to the optical axis (5) and slightly inferior. The eye has to rotate to a tilted position in relation to the optical axis to allow the refracted light rays to fall on the fovea (see Figure 1a). Consequently, the eye becomes oriented in such a way that its visual axis aligns with the topographer's axis, resulting in tilted Scheimpflug images and tilted topography maps in relation to its geometrical centre (6), Figure 1b. Accurately compensating for this induced tilt is challenging as the eye's surface has few distinguishable features (7).

While the optical axis could be considered as a perfect representation of the geometrical axis of the eye as it represents, in theory, the path of a light ray that enters and leaves the optical system of the eye along the same line (8), such a path may never exist in actual eyes. Even if there is a unique optical axis for a human eye, the fact that this axis meets the retina nasally below the fovea, missing its central sensitive zone (9), makes it difficult to be identified clinically (10). However, while the eye's optical axis may be a theoretical construct, which does not exist in the real-world (11), the axis remains an important reference line for the measurement and analysis of ocular shape. Its applications include being a geometrical axis for spectacles (12) and other corrective lenses that are manufactured in processes that require a unique geometrical centreline like a lathe centred on its spindles (13) or an injection moulding machine where centring the two halves of the mould around a geometrical axis is an essential process (14). Another application is in computer-based eye modelling systems that trace light rays

through the ocular system (15). These systems reconstruct the eye shape while relying on a coordinate system based on a common axis (16). As in these models, the angle between the visual axis and the optical axis is relatively small, it is common to treat these two axes equally (17), even though this treatment can lead to alignment errors in vision-correction products like multifocal contact lenses, where centration over the patient's visual axis is essential for adequate optical performance (18).

Accepting the argument that the eye possibly has no perfect axis of symmetry (19) and no true optical axis (20), this study considers the geometrical axis of the eye as (a) the optimal line that minimises the asymmetric shape deviation of the ocular system's anterior components, (b) the line that offers the most satisfactory axis adopted in manufacturing spectacles and contact lenses, and (c) the centreline that can be used as a reference in modelling applications in computer aided design (CAD) or finite element (FE) modelling packages. The study presents a methodology to level the eye's topography data, making it normal to its optimal geometrical axis, thus providing a specific engineering design information regarding human ocular shape. Hence, the study presents the geometrical axis that passes through the geometric centre of the cornea and the mean distance between this axis and the visual axis in fellow eyes for three different populations.

Subjects and Methods

Clinical data

The ethics committee of the Federal University of São Paulo (Brazil) approved this retrospective research study, which was conducted in accordance with the standards set in the 1964 Declaration of Helsinki, and its revisions till Fortaleza 2013. Due to the reported topographical and anatomical differences between ethnic groups (21-23), it was decided that the study should

look at different populations and investigate if results were attached to a certain population. The study involved scanning both eyes of 181 Brazilian (aged 35.6 ± 15.8), 500 Chinese (aged 24.2 ± 5.7) and 343 Italian (aged 37.6 ± 13.5) participants selected from referrals to Instituto de Olhos Renato Ambrósio (Rio de Janeiro, Brazil), the Wenzhou Eye Hospital (Wenzhou, China), and Vincieye Srl Eye Clinic (Milan, Italy) respectively.

Before being anonymised, clinical topography data has been collected from both eyes of normal participants from three populations in three different countries using the Pentacam HR[®] (OCULUS Optikgeräte GmbH, Wetzlar, Germany). Participants from Brazil, China and Italy, with no history of ocular disease, trauma or ocular surgery, were selected. Those with intraocular pressure (IOP) higher than 21 mmHg as measured by the Goldmann Applanation Tonometer, soft contact lens wear until less than two weeks before measurement, or rigid gas-permeable (RGP) contact lens wear until less than four weeks before measurements were excluded. Pentacam HR elevation data for the anterior surface were exported in comma-separated values (CSV) format and analysed using custom-built Matlab[®] (MathWorks, Natick, USA) codes.

Determination of corneal tilt

Corneal topography data collected by a topographer usually have the eye's visual axis aligned with the topography machine's axis, with the eye becoming tilted because of this alignment. This tilt is compensated such that the geometrical axis becomes the reference line of the data instead of the visual axis.

The process of levelling the topography data starts with considering the raw Pentacam HR elevation data, which is available in a Cartesian form:

$$X = x_1, x_2, x_3, \dots, x_n \quad \text{Equation 1}$$

$$\langle i \rangle Y = y_1, y_2, y_3, \dots y_n \langle /i \rangle \quad \text{Equation 2}$$

$$\langle i \rangle Z = z_1, z_2, z_3, \dots z_n \langle /i \rangle \quad \text{Equation 3}$$

From the X and Y coordinate data, the polar radius of each point ($\langle i \rangle r \langle /i \rangle$) is obtained as:

$$\langle i \rangle r_p = \sqrt{X^2 + Y^2} \langle /i \rangle \quad \text{Equation 4}$$

which is then normalised to fit within a unit circle by dividing $\langle i \rangle r_p \langle /i \rangle$ for each point by the maximum polar radius value across the measured corneal surface:

$$\langle i \rangle r = \frac{r_p}{r_{p_{\max}}} \langle /i \rangle \quad \text{Equation 5}$$

On the other hand, the polar angular position array, $\langle i \rangle \theta \langle /i \rangle \langle i \rangle, \langle /i \rangle$ is calculated from the inverse trigonometric function

$$\langle i \rangle \theta = \tan^{-1} \frac{Y}{X} \langle /i \rangle \quad \text{Equation 6}$$

using the right-hand rule, which defines the positive direction of the angle $\langle i \rangle \theta \langle /i \rangle$.

With this manipulation, the cornea's elevation data ($\langle i \rangle r \langle /i \rangle$ and $\langle i \rangle \theta \langle /i \rangle$) is fitted to first-order Zernike polynomial (24), $\langle i \rangle Z_{\text{Zernike}} \langle /i \rangle$, in the form

$$\langle i \rangle Z_{\text{Zernike}} = C_1 - C_2 r \sin \theta + C_3 r \cos \theta \langle /i \rangle \quad \text{Equation 7}$$

where Zernike coefficients $\langle i \rangle C_1 \langle /i \rangle$, $\langle i \rangle C_2 \langle /i \rangle$ and $\langle i \rangle C_3 \langle /i \rangle$ represent the respective contribution of the piston, vertical tilt and horizontal tilt to the fitted corneal surface (25), Figure 2. The Zernike polynomials were first described by Zernike (26) and widely used to describe the complex shape of the human corneal surface through the values of their terms and coefficients (27). They are sets of polynomials function of two variables, radius (r) and angular position (θ) that are orthogonal inside a unit circle (circle with a radius of one). Through using Zernike

polynomials, the eye surface can be constructed from the combination of terms that have a physical meaning directly commented to the ocular surface characteristics. The first term in a typical first-order (maximum power of r equals one) Zernike polynomial (Equation 7) is called the piston. The piston is a term represents the mean value of the fitted corneal surface and, as appeared from its name, performs like an engine piston moving up and down according to the topography of each individual eye. The next two terms of the Zernike polynomial are representing the vertical tilt of the fitted surface around the X-axis (superior-inferior) and the horizontal tilt around the Y-axis (nasal-temporal) where the Z-axis is considered as the line coming out from the corneal apex perpendicular to its surface. Therefore, fitting a corneal surface to a first-order Zernike polynomial enables the determination of the tilt coefficients around the X-axis (C_2) and the Y-axis (C_3), Figure 2. The levelling strategy adopted was to rotate the corneal surface around X- axes and Y-axes by angles α_x and α_y , respectively, in order to minimise the Zernike tilt coefficients C_2 and C_3 . The three-dimensional rotation was achieved by adopting the following three rotation matrices (28), in which the rotation angle about Z-axis, α_z , was set to zero.

$$R_x(\alpha_x) = \begin{bmatrix} 1 & 0 & 0 \\ 0 & \cos \alpha_x & -\sin \alpha_x \\ 0 & \sin \alpha_x & \cos \alpha_x \end{bmatrix} \quad \text{Equation 8}$$

$$R_y(\alpha_y) = \begin{bmatrix} \cos \alpha_y & 0 & \sin \alpha_y \\ 0 & 1 & 0 \\ -\sin \alpha_y & 0 & \cos \alpha_y \end{bmatrix} \quad \text{Equation 9}$$

$$R_z(\alpha_z) = \begin{bmatrix} \cos \alpha_z & -\sin \alpha_z & 0 \\ \sin \alpha_z & \cos \alpha_z & 0 \\ 0 & 0 & 1 \end{bmatrix} \quad \text{Equation 10}$$

Following the elemental rotation rule, the rotated coordinates X_r , Y_r and Z_r were calculated as:

$$\langle i \rangle \begin{bmatrix} X_{r1} & X_{r2} & X_{r3} & \dots & X_{rn} \\ Y_{r1} & Y_{r2} & Y_{r3} & \dots & Y_{rn} \\ Z_{r1} & Z_{r2} & Z_{r3} & \dots & Z_{rn} \end{bmatrix}$$

Equation 11

$$= [R_x(\alpha_x) * R_y(\alpha_y) * R_z(\alpha_z)] * \begin{bmatrix} X_1 & X_2 & X_3 & \dots & X_n \\ Y_1 & Y_2 & Y_3 & \dots & Y_n \\ Z_1 & Z_2 & Z_3 & \dots & Z_n \end{bmatrix} \langle /i \rangle$$

The optimisation looping procedure was set to end when the absolute values of both of Zernike coefficients, $\langle i \rangle C_2 \langle /i \rangle$ and $\langle i \rangle C_3 \langle /i \rangle$ became close to zero. This process was carried out by the Levenberg-Marquardt nonlinear least squares algorithm (LMA) (29) via the Matlab Optimisation Toolbox.

LMA is a standard iterative procedure process rediscovered by Marquardt and published by Levenberg (30). It is a robust technique for solving nonlinear curve fitting problems by searching for a solution (tilt angles $\langle i \rangle \alpha_x \langle /i \rangle$ and $\langle i \rangle \alpha_y \langle /i \rangle$) that minimise the values of Zernike coefficients, $\langle i \rangle C_2 \langle /i \rangle$ and $\langle i \rangle C_3 \langle /i \rangle$ to a pre-set value. In this study, the LMA algorithm was set to stop the optimisation process when both Zernike coefficients are below $\langle i \rangle 10^{-20} \langle /i \rangle$. The optimisation process for each eye's topography produced the optimal values of the rotation angles $\langle i \rangle \alpha_x \langle /i \rangle$ and $\langle i \rangle \alpha_y \langle /i \rangle$ which can be used to level the topography map such that its geometrical axis became parallel to the Z-axis, Figure 4. Tilt angles $\langle i \rangle \alpha_x \langle /i \rangle$ around X-axis and $\langle i \rangle \alpha_y \langle /i \rangle$ around Y-axis were then compared statistically for each of the three populations involved in the presented study where the significance of the differences between the tilt in different directions was calculated, Figure 5. Using the geometrical axis (Z-axis) as a reference, the position of the visual axis of the anterior corneal surface (visual centre) was located and plotted graphically in Figures 6 to 8. To allow an efficient comparison between the right and left eyes among the participants of this study, the zero-angular position was located on the nasal side of each eye. The polar coordinate angular nil position was taken at

the 3 O'clock position for the right eyes with counter clockwise positive direction, and 9 O'clock position for left eyes with clockwise positive direction.

Statistical analysis

Statistical analysis was performed using Matlab Statistics and Machine Learning Toolbox (MathWorks, Natick, USA). The null hypothesis probability (p) at 95% at confidence level was calculated. Two sample t-test was used to investigate the significance between pairs of data sets to check whether the results represent independent record. The probability p is an element of the period $[0, 1]$ where values of p higher than 0.05 indicates the validity of the null hypothesis (31).

Results

The current study results showed that topography levelling values for the data taken with the Pentacam HR were significantly different in right and left eyes as can be seen in Figure 5. Statistical analysis showed that the differences between the vertical and horizontal tilt angles (α_x, α_y) were significant among Brazilian, Chinese and Italian participants ($p < 0.001$). Likewise, comparing the tilt angles between fellow eyes of individuals in each group showed significant differences between right and left eyes ($p < 0.001$) among the three investigated groups, Table 2. Vertical and horizontal average difference absolute values between right and left eyes were $-0.90 \pm 2.24^\circ$ and $1.45 \pm 1.71^\circ$ among Brazilian participants, $-0.57 \pm 1.68^\circ$ and $1.69 \pm 1.27^\circ$ among Chinese participants, $-1.63 \pm 2.14^\circ$ and $3.00 \pm 2.33^\circ$ in Italian participants. The mean absolute differences in the vertical tilt angles between the Chinese and the Brazilian participants were 2.1° , 2.2° for right and left eyes respectively, however, these mean absolute differences were 0.9° , 2.0° between the Chinese and the Italian participants. The trend of mean absolute differences in horizontal tilt angles was the same as absolute differences in horizontal

tilt angles but with less variation. Mean absolute differences were 0.7° , 0.8° for right and left eyes respectively between the Chinese and the Brazilian participants and 2.0° , 0.6° between the Chinese and the Italian participants.

Using polar coordinates, the radial distance, r , and the angular position, ϕ , between the geometrical axis and the visual centre, varied significantly between right and left eyes of participants within the same population. As can be seen in Table 1, the visual centres of right eyes were slightly farther from the geometrical centres than left eyes in all three groups. The mean distances varied from 0.02 mm in Brazilian participants to 0.11 mm in Chinese participants and 0.16 mm in Italian participants. On the other hand, the angular positions of the visual axes of right eye were consistently lower than left eyes with differences of 20.7° , 27.6° and 38.6° among Brazilian, Chinese and Italian participants, respectively. Figures 5 to 7 show the mean positions of visual centres in Brazilian participants (Figure 6), Chinese participants (Figure 7) and Italian participants (Figure 8).

Discussion

The challenges in determining corneal topography tilt and the position of the visual axis include the accurate determination of the geometrical axis. This challenge was met in this study by using a three-dimensional rotation technique combined with a topography fit to first-order Zernike polynomials and a nonlinear least-squares optimisation function. This methodology was adopted despite uncertainty with respect to the existence of a true rotational symmetry axis in the human eye (32) since an optimal geometrical axis is needed for practical reasons such as design and fitting of prescription glasses and contact lenses.

Using this methodology, the results revealed some consistent characteristics related to the position of the human eye's visual centre. In all eyes considered, the visual centre was located

in the nasal-superior direction relative to the geometrical axis. This finding matches the temporal-inferior location of the human fovea (33) and the fact that opposite direction rotation is required for a clear vision of a short-distance target. It is also in line with evidence that the pupil centre is located temporally and frequently infero-temporally relative to the coaxially sighted corneal light reflex (34).

However, the data pointed at different performance of right and left eyes during the fixation process – with right eyes tending to rotate more than left eyes, the differences in tilt angles between fellow eyes were significant in all three participant groups ($p < 0.001$). Again, this finding is compatible with the facts that (a) right and left eyes commonly differ in their dioptric powers and astigmatic axes, (b) two-thirds of the population are believed to be right-eye dominant (32, 35-38), (c) the vision field of right eyes is different from that of left eyes (38), and (d) the image merging processes carried out within the brain for the two eyes are different (40, 41). These differences effectively require different performance of the two eyes during the fixation process (42) and help explain why our data suggests that the participants' right eyes were more dynamic during the fixation process and therefore, the distance between the visual centre and geometrical axis in the right eyes were longer than in the left eyes.

It should also be considered that the human eye sees objects upside-down with a blind spot caused by the optic nerve head connection to the retina (43). Correcting the orientation of the images produced by the eyes, and merging them in a way that bridges the gap caused by the blind spot, may require slightly different orientation of the two eyes to achieve the best results.

As simplified representations of the human eye usually ignore the effect of hemispheric division of the brain on the eye position (44), some of the outcomes of such representations do not reflect the eye's behaviour in the real-world (45, 46). Therefore, the levelling method presented

in this paper should provide an effective way for eye modellers to adopt the correct orientation of topography data in their eye mathematical models. The method should further support multifocal contact lenses designers who are interested in making the centre of their lenses' optical axis aligned with the eye's visual axis.

The study showed that the average eye tilt was varying less between the Brazilian and the Italian populations for both right and left eyes however, it was notably less among Chinese population compared to the other two populations. It was also clear from the results that position of the visual centre is more close to the geometrical centre among the Chinese population compared to the Brazilian and the Italian populations. These results were in-line with the reported topographical and anatomical differences between Caucasian and Chinese ethnic groups (21-23), were the majority of the Brazilian and the Italian participants in this study could be considered as Caucasian.

In conclusion, the study presented a method based on using first order Zernike polynomial fitting and an optimisation technique to level corneal topography data normal to the cornea's geometrical axis. By achieving this goal, the study demonstrated that right eyes tend to rotate temporally by $2\pm 2^\circ$ and inferiorly by $1\pm 2^\circ$ more than left eyes during the fixation process. The study also showed that the visual centres of fellow eyes are not symmetrically located – the centres were slightly farther from the geometrical centre (0.12 ± 0.26 mm) and more nasally oriented ($30\pm 40^\circ$) in right eyes compared to the left eyes. The study showed that the eye tilt during the topography scan was a general trend among participants from the three investigated populations, the phenomena among the Chinese population was slightly less compared to the Brazilian and the Italian populations.

The findings of the study can be used to improve the quality of applications that rely on the use of corneal topography data, such as contact lenses fitting, corneal implant design and refractive surgery planning. The positioning of the geometrical axis can further improve accuracy in locating the keratoconus cone or orientating the astigmatism axis for individual patients.

Declaration of interest

All authors of this article declare that they have no conflict of interest.

References

1. Cox C. Physical Assessment for Nurses. UK: John Wiley & Sons; 2009. 418 p.
2. Yao Ni, Xia-Lin Liu, Ming-Xing Wu, Ying Lin, Yu-Ying Sun, Chang He, and Yi-Zhi Liu. Objective evaluation of the changes in the crystalline lens during accommodation in young and presbyopic populations using Pentacam HR system. Int J Ophthalmol. 2011; 4(6): 611-615.
3. Applegate RA, Thibos LN, Twa MD, Sarver EJ. Importance of fixation, pupil center, and reference axis in ocular wavefront sensing, videokeratography, and retinal image quality. J Cataract Refract Surg. 2009;35(1):139-52.
4. Kolb H FE, Nelson R. Facts and Figures Concerning the Human Retina. System WTOotRaV, editor. Salt Lake City (UT): University of Utah Health Sciences Center; 1995.
5. Gross H. Handbook of optical systems. 4. Weinheim: Wiley-VCH; 2005.
6. de Castro A, Rosales P, Marcos S. Tilt and decentration of intraocular lenses in vivo from Purkinje and Scheimpflug imaging: Validation study. J Cataract Refract Surg. 2007;33(3):418-29.

7. Harris WF. Optical axes of catadioptric systems including visual, Purkinje and other nonvisual systems of a heterocentric astigmatic eye. *S Afr Optom.* 2010;69(3):152-60.
8. Arba Mosquera S, Verma S, McAlinden C. Centration axis in refractive surgery. *Eye Vis (Lond).* 2015;2:4.
9. Yang Q, Cho KS, Chen H, Yu D, Wang WH, Luo G, et al. Microbead-induced ocular hypertensive mouse model for screening and testing of aqueous production suppressants for glaucoma. *Invest Ophthalmol Vis Sci.* 2012;53(7):3733-41.
10. Thibos LN, Bradley A, Still DL, Zhang X, Howarth PA. Theory and measurement of ocular chromatic aberration. *Vision Res.* 1990;30(1):33-49.
11. Schwiegerling JT. Eye axes and their relevance to alignment of corneal refractive procedures. *J Refract Surg.* 2013;29(8):515-6.
12. Rosenthal JW. *Spectacles and Other Vision Aids: A History and Guide to Collecting.* USA: Norman Pub.; 1996.
13. Hmt HMTB. *Production Technology.* India: McGraw-Hill Education (India) Pvt Limited; 2001.
14. Goodship V, Arburg. *Practical Guide to Injection Moulding.* UK: Rapra Technology; 2004.
15. Ng EYK, Tan JH, Acharya UR, Suri JS. *Human Eye Imaging and Modeling.* USA: Taylor & Francis; 2012.
16. Komzsik L. *What Every Engineer Should Know about Computational Techniques of Finite Element Analysis.* 2 ed. USA: CRC Press; 2016.
17. Ward NJ, Ho KW, Lambert WS, Weitlauf C, Calkins DJ. Absence of transient receptor potential vanilloid-1 accelerates stress-induced axonopathy in the optic projection. *J Neurosci.* 2014;34(9):3161-70.

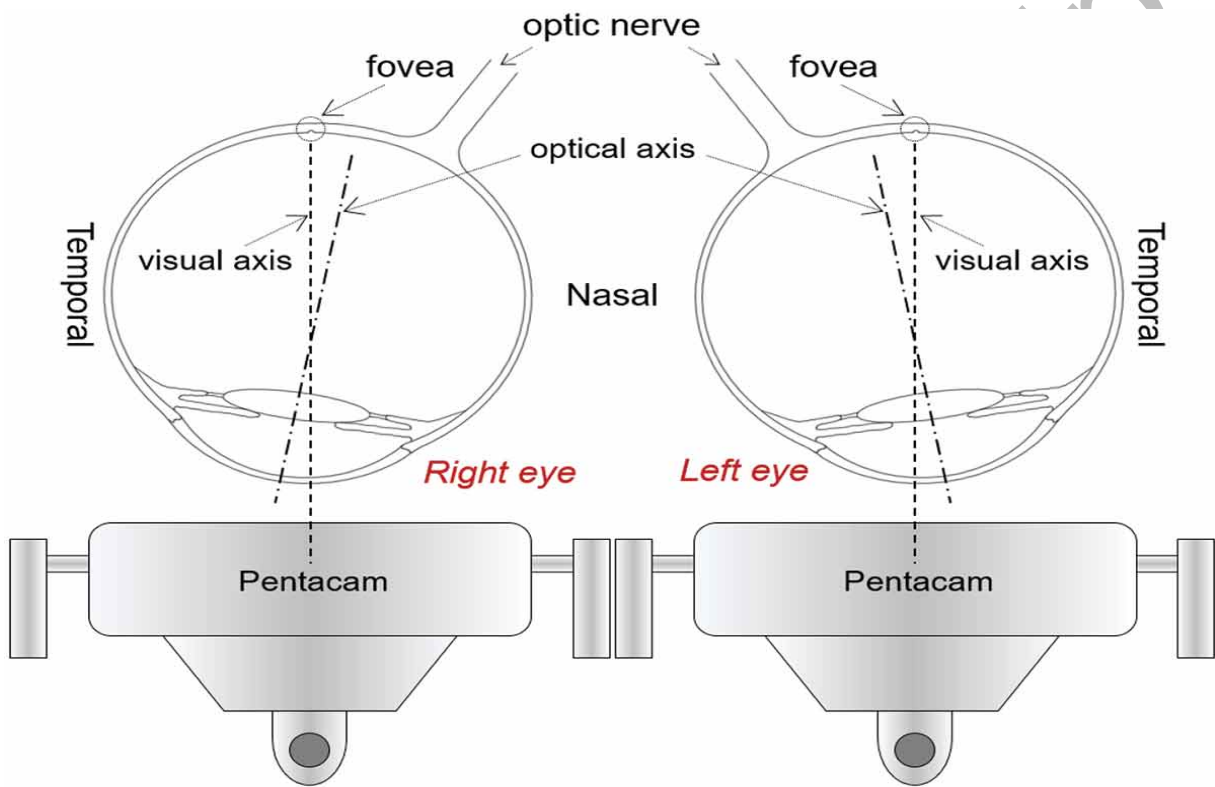
18. Davis RL. Determining Multifocal Parameters for a Better Fit. *Review of Optometry*. 2016;153(8):50-5.
19. Navarro R. The Optical Design of the Human Eye: a Critical Review. *J Optom*. 2009;2(1):3-18.
20. Harris WF. Optical Axes of Eyes and Other Optical Systems. *Optom Vis Sci*. 2009;86(5):537-41.
21. Hickson-Curran S, Brennan NA, Igarashi Y, Young G. Comparative evaluation of Asian and white ocular topography. *Optom Vis Sci*. 2014;91(12):1396-405.
22. Hickson-Curran S, Young G, Brennan N, Hunt C. Chinese and Caucasian ocular topography and soft contact lens fit. *Clin Exp Optom*. 2016;99(2):149-56.
23. Lam CSY, Loran DFC. Designing contact lenses for oriental eyes *Cont Lens Anterior Eye*. 1991;14(3):109-14.
24. Malacara D. *Optical Shop Testing*. USA: Wiley; 2007.
25. Jagerman LS. *Ophthalmologists, Meet Zernike and Fourier!* Canada: Trafford Publishing; 2007. 99 p.
26. F. Zernike, Beugungstheorie des schneidenverfahrens und seiner verbesserten form, der phasenkontrastmethode, *Physica*1934; 7-12(1): 689-704.
27. Thibos LN, Applegate RA, Schwiegerling JT, Webb R; VSIA Standards Taskforce Members. Vision science and its applications. *J Refract Surg*. 2002;18(5):652-60.
28. Arvo J. Fast random rotation matrices. In: David K, editor. *Graphics Gems III*. USA: Academic Press Professional, Inc.; 1992. p. 117-20.
29. Guyon F, Riche RL. *Least Squares Parameter Estimation and the Levenberg-Marquardt Algorithm: Deterministic Analysis, Sensitivities and Numerical Experiments*. France: INSA de Rouen; 1999.

30. Levenberg K. A Method for the Solution of Certain Non-Linear Problems in Least Squares. *Quart. Appl. Math.* 2 (1944), 164-168
31. Everitt BS, Skrondal A. *The Cambridge Dictionary of Statistics*. Cambridge, UK: Cambridge University Press; 2010.
32. Dai G. *Wavefront Optics for Vision Correction*. Dai G-m, editor. USA: Society of Photo Optical; 2008.
33. Jonas RA, Wang YX, Yang H, Li JJ, Xu L, Panda-Jonas S, et al. Optic Disc - Fovea Angle: The Beijing Eye Study 2011. *PLoS One*. 2015;10(11):e0141771.
34. Erdem U, Muftuoglu O, Gundogan FC, Sobaci G, Bayer A. Pupil center shift relative to the coaxially sighted corneal light reflex under natural and pharmacologically dilated conditions. *J Refract Surg*. 2008;24(5):530-8.
35. Chaurasia BD, Mathur BB. Eyedness. *Acta Anat (Basel)*. 1976;96(2):301-5.
36. Reiss MR. Ocular dominance: some family data. *Laterality*. 1997;2(1):7-16.
37. Ehrenstein WH, Arnold-Schulz-Gahmen BE, Jaschinski W. Eye preference within the context of binocular functions. *Graefes Arch Clin Exp Ophthalmol*. 2005;243(9):926-32.
38. Eser I, Durrie DS, Schwendeman F, Stahl JE. Association between ocular dominance and refraction. *J Refract Surg*. 2008;24(7):685-9.
39. Siegel A, Sapru HN. *Essential Neuroscience*. China: Lippincott Williams & Wilkins; 2006.
40. Lefebvre E. *Advances and Challenges in Multisensor Data and Information Processing*. Netherlands: IOS Press; 2007. 401 p.
41. Barro S, Marin R. *Fuzzy Logic in Medicine*. Spain: Physica-Verlag HD; 2013.
42. Bergamin O, Straumann D. Three-Dimensional Binocular Kinematics of Torsional Vestibular Nystagmus During Convergence on Head-Fixed Targets in Humans. *J Neurophysiol*. 2001;86(1):113-22.

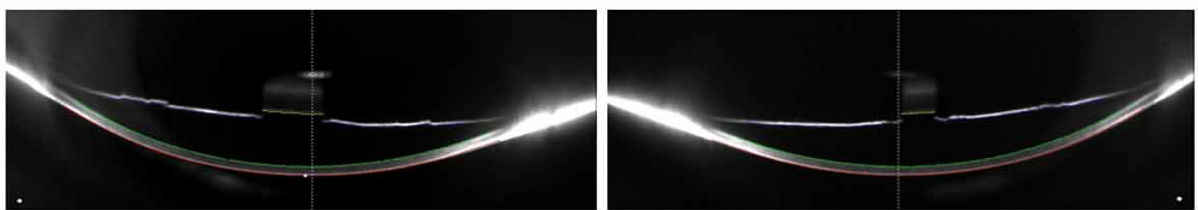
43. Cai Y. Instinctive Computing. UK: Springer London; 2017.
44. Polpitiya AD, Dayawansa WP, Martin CF, Ghosh BK. Geometry and Control of Human Eye Movements. IEEE Transactions on Automatic Control. 2007;52(2):170-80.
45. Davelaar EJ. Connectionist Models of Neurocognition and Emergent Behavior: From Theory to Applications. Singapore: World Scientific Publishing Company; 2012.
46. London A, Benhar I, Schwartz M. The retina as a window to the brain - from eye research to CNS disorders. Nat Rev Neurol. 2013;9(1):44-53.

Accepted Manuscript

Figure 1: (a) The tilted eye position to allow focused light rays to fall on the fovea during the topography scanning process (b) Pentacam HR Scheimpflug images for an Italian participant, 75 years old female, showing horizontal cross-sectional views of right and left eyes during the topography scan.



(a)

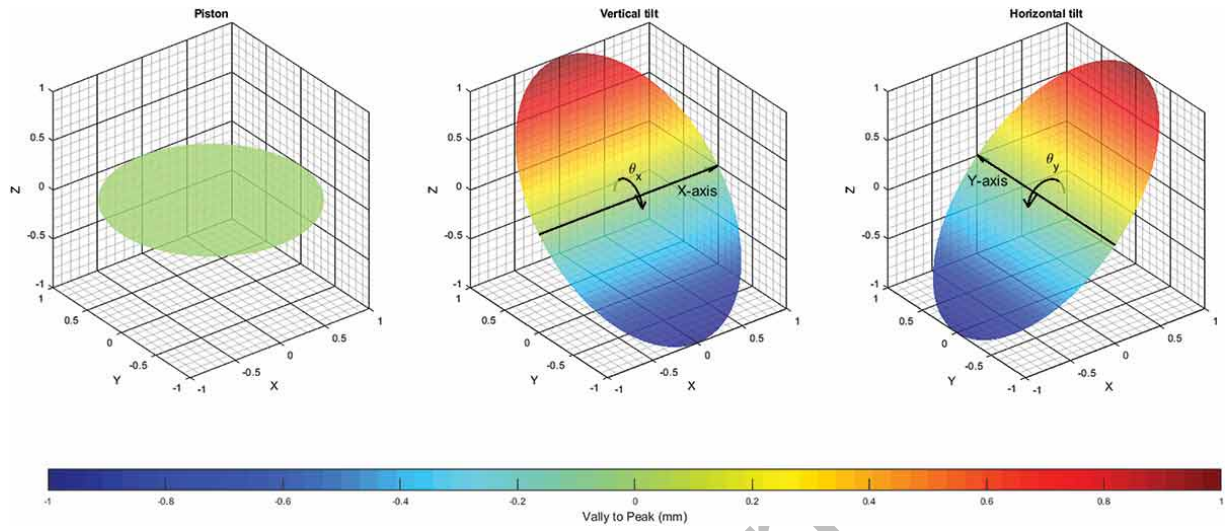


Right eye

Left eye

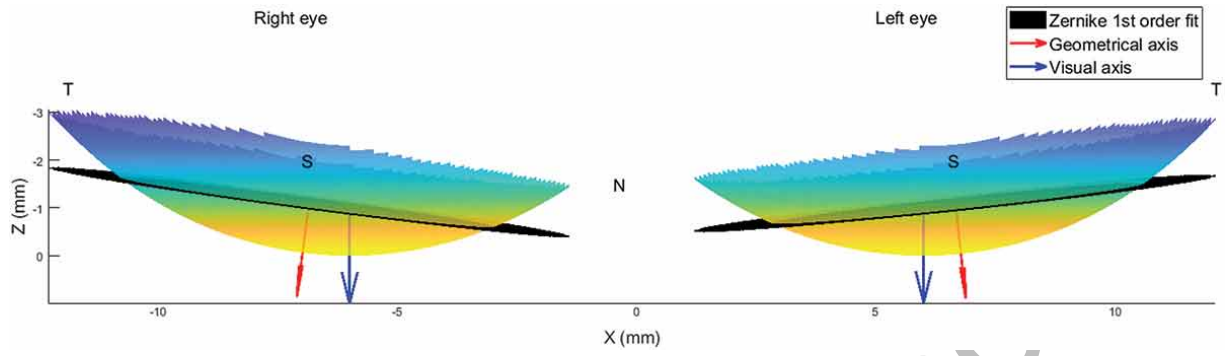
(b)

Figure 2: Graphical representation of first-order Zernike polynomial terms.



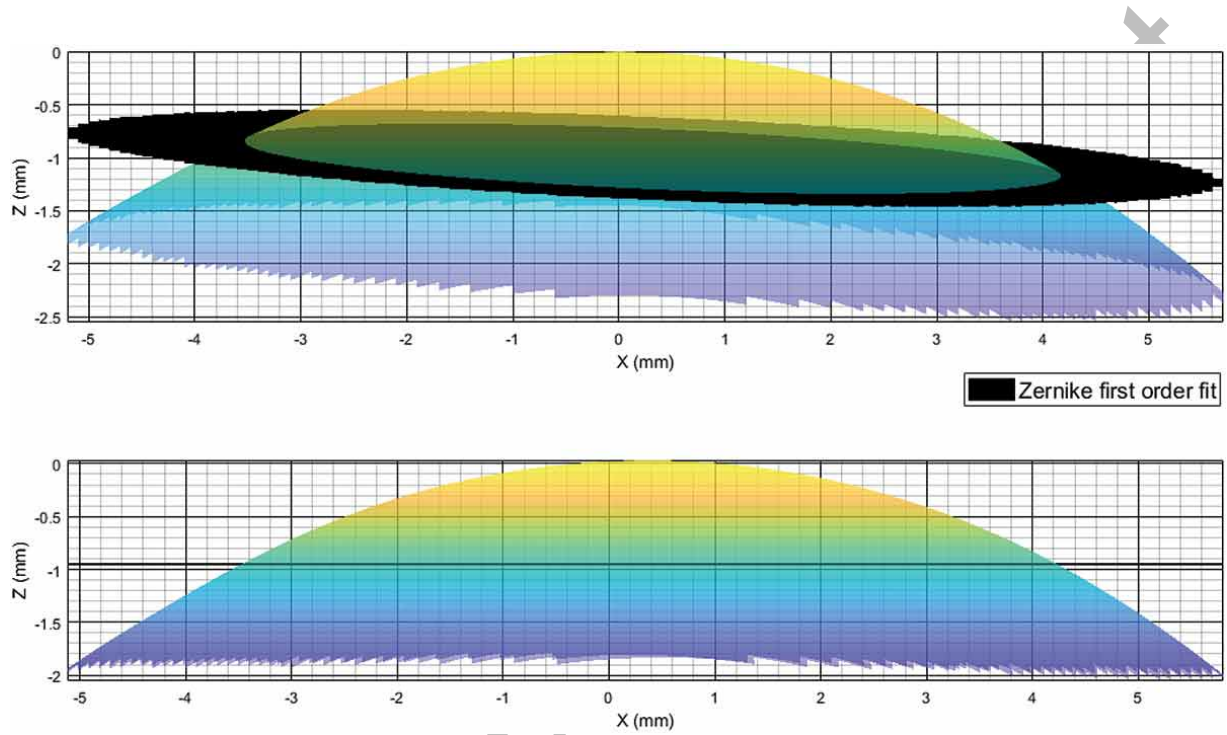
Accepted Manuscript

Figure 3: Determining corneal tilt by first-order Zernike polynomial fit (Same participant as in Figure 1b).



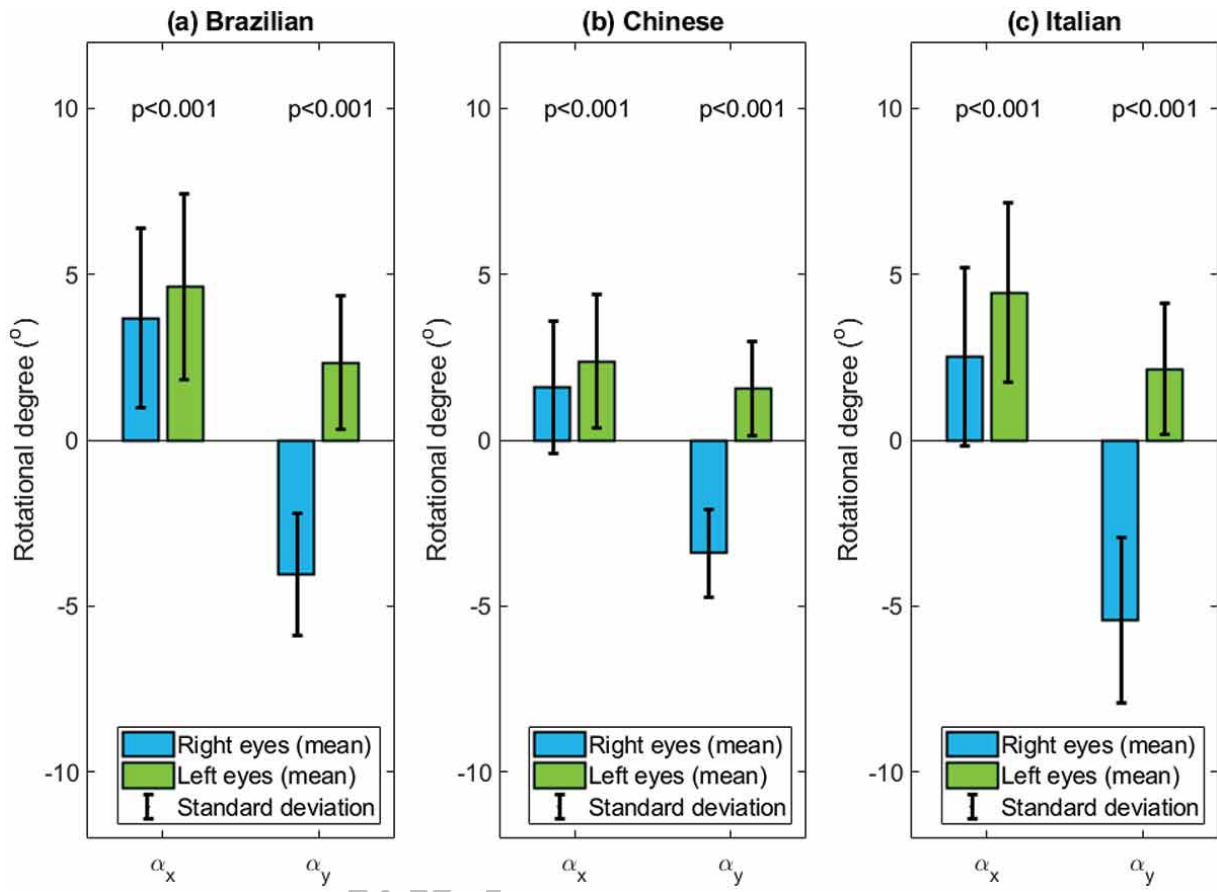
Accepted Manuscript

Figure 4: Left eye an Italian participant, same participant as in Figures 3 and 5. (a) As measured by the Pentacam HR where the first-order Zernike fitted surface shown in black. (b) After being levelled by Zernike first-order fit. In this case rotation angles were $\alpha_x = -4.4^\circ$ and $\alpha_y = -2.6^\circ$.



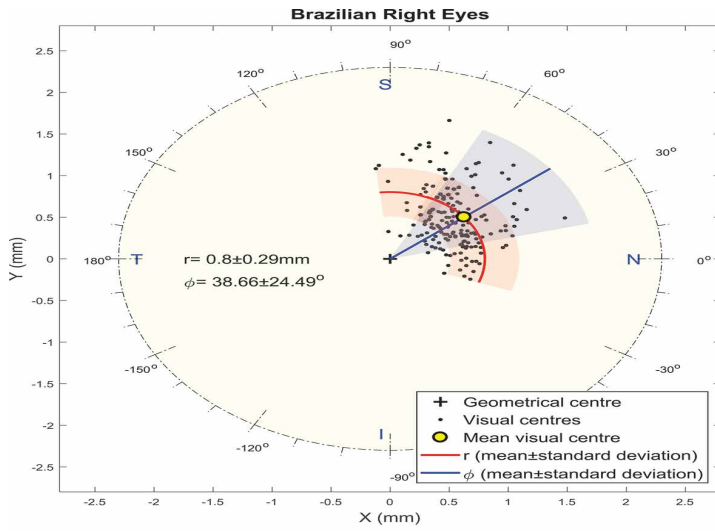
Accepted

Figure 5: Vertical and horizontal tilt angles among participants involved in this study.

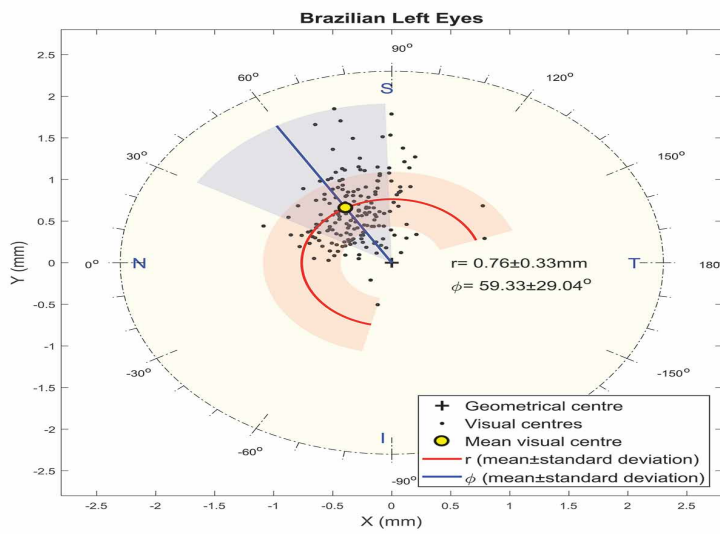


Accepte

Figure 6: Brazilian corneal visual centre position (a) right eyes (b) left eyes.

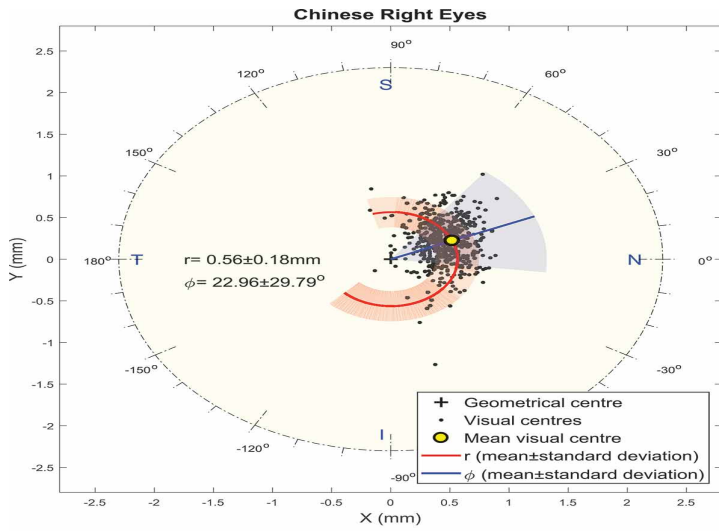


(a)

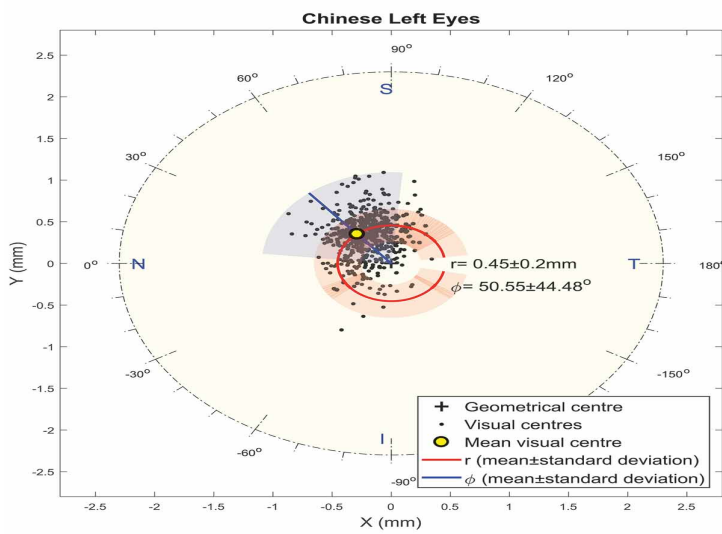


(b)

Figure 7: Chinese corneal visual centre position (a) right eyes (b) left eyes.

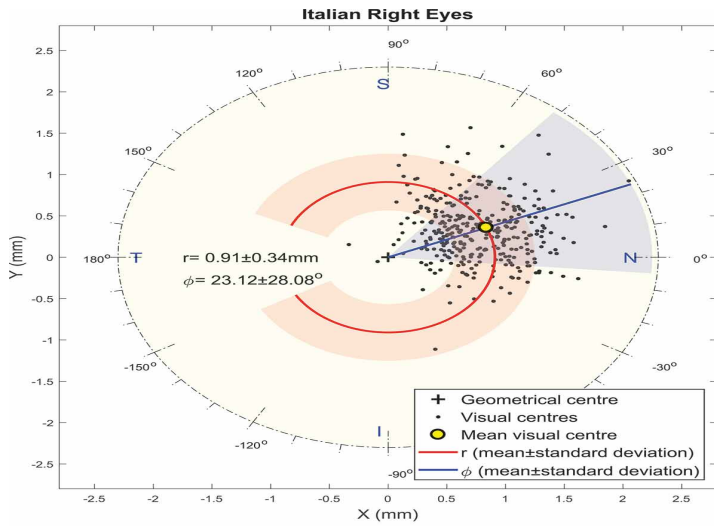


(a)

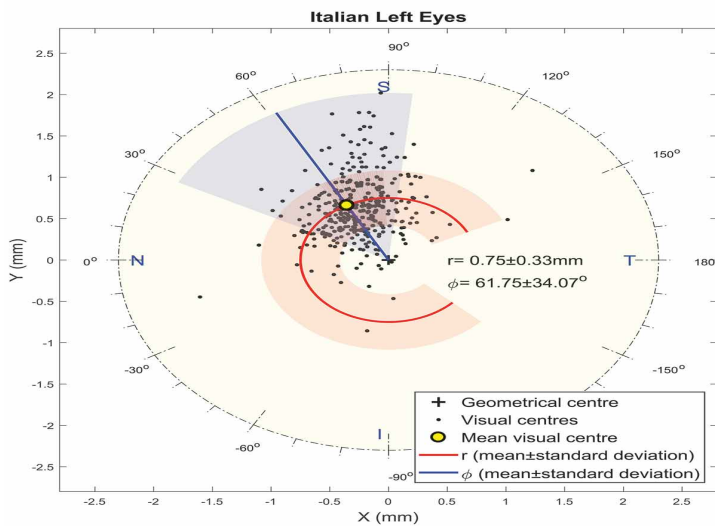


(b)

Figure 8: Italian corneal visual centre position (a) right eyes (b) left eyes.



(a)



(b)

Table 1: Position of the visual centre relative to the geometrical axis in the three participant groups

Brazilian participants		Chinese participants		Italian participants	
r (mm)	ϕ (°)	r (mm)	ϕ (°)	r (mm)	ϕ (°)

Right eyes						
mean ± SD	0.8022 ± 0.2915	38.659 ± 24.4909	0.5643 ± 0.1811	22.9582 ± 29.7947	0.9093 ± 0.3420	23.1244 ± 28.0798
min : max	0.289 : 1.7364	-20.672 : 96.386	0.0159 : 1.3194	-134.2652 : 106.6232	0.1037 : 2.2476	-149.9255 : 155.3999
Left eyes						
mean ± SD	0.7631 ± 0.3283	59.3315 ± 29.036	0.4531 ± 0.1995	50.5526 ± 44.4763	0.7495 ± 0.3342	61.7530 ± 34.0705
min : max	0.1445 : 1.9122	-76.708 : 159.6492	0.0396 : 1.0944	-168.0463 : 171.3125	0.0363 : 2.0205	-136.5978 : 154.2798

Table 2: Eye's vertical and horizontal tilts in the three participant groups.

Table 2: Eye's **vertical and horizontal** tilts in the three participant groups

	Brazilian participants			Chinese participants			Italian participants		
	Right eyes	Left eyes	<i>p</i>	Right eyes	Left eyes	<i>p</i>	Right eyes	Left eyes	<i>p</i>
Vertical tilt angle (α_x°)									
mean ± SD	3.6773 ± 2.7109	4.6304 ± 2.8012	<0.001	1.5818 ± 2.0035	2.3752 ± 2.0278	<0.001	2.5152 ± 2.6782	4.4458 ± 2.7185	<0.001
min : max	-1.7347 : 11.8390	-3.6901 : 14.1928		-8.6539 : 7.0852	-5.8678 : 8.2655		-8.4828 : 11.0971	-6.3511 : 13.1685	
Horizontal tilt angle (α_y°)									
mean ± SD	-4.0561 ± 1.8354	2.3385 ± 2.0101	<0.001	-3.4079 ± 1.3159	1.5468 ± 1.4119	<0.001	-5.4237 ± 2.4978	2.1375 ± 1.9672	<0.001
min : max	-10.9288 : 0.8254	-6.7956 : 7.7276		-6.9106 : 1.4883	-2.4316 : 6.6351		-13.8360 : 2.4202	-8.3381 : 7.8195	
<i>p</i>	<0.001	<0.001		<0.001	<0.001		<0.001	<0.001	